MAPK signaling couples SCF-mediated degradation of translational regulators to oocyte meiotic progression

Edyta Kisielnicka[a], Ryuji Minasaki[a], and Christian R. Eckmann[a,1]

[a]Developmental Genetics, Institute of Biology, Martin Luther University Halle-Wittenberg, 06120 Halle (Saale), Germany

Edited by David Greenstein, University of Minnesota, Minneapolis, MN, and accepted by Editorial Board Member Trudi Schüpbach January 31, 2018 (received for review September 1, 2017)

RNA-binding proteins (RBPs) are important regulators of gene expression programs, especially during gametogenesis. How the abundance of particular RBPs is restricted to defined stages of meiosis remains largely elusive. Here, we report a molecular pathway that subjects two nonrelated but broadly evolutionarily conserved translational regulators (CPB-3/CPEB and GLD-1/STAR) to proteosomal degradation in *Caenorhabditis elegans* germ cells at the transition from pachytene to diplotene of meiotic prophase. Both RBPs are recognized by the same ubiquitin ligase complex, containing the molecular scaffold Cullin-1 and the tumor suppressor SEL-10/FBXW7 as its substrate recognition subunit. Destabilization of either RBP through this Skp, Cullin, F-box–containing complex (SCF) ubiquitin ligase appears to loosen its negative control over established target mRNAs, and presumably depends on a prior phosphorylation of CPB-3 and GLD-1 by MAPK (MPK-1), whose activity increases in mid- to late pachytene to promote meiotic progression and oocyte differentiation. Thus, we propose that the orchestrated degradation of RBPs via MAPK-signaling cascades during germ cell development may act to synchronize meiotic with sexual differentiation gene expression changes.

germ cell development | RNA-binding proteins | Erk kinase signaling | F-box proteins | ubiquitin ligase complex

Gametogenesis relies on the execution of two developmental programs that run in parallel: the stepwise completion of consecutive meiotic phases to produce haploid nuclei and the synchronized differentiation of immature germ cells into sexually dimorphic gametes. This synchronization is particularly apparent in developing oocytes, in which meiotic progression halts at defined stages to support cell growth and other cell-type specific changes (1, 2). Periods of meiotic arrest are primarily lifted by external cues, such as hormonal stimulation or fertilization (3). Thus, gene expression programs that drive and coordinate meiotic cell divisions with germ cell differentiation must be connected to regulatory pathways, ensuring tight developmental synchrony.

Particularly during oogenesis, gene expression programs are predominantly regulated at the posttranscriptional level due to strongly reduced transcriptional activities (3, 4). During their development, oocytes accumulate a wide range of mRNAs, which may remain translationally silent for a long time, until a signaling event triggers their translational de-repression (3, 4). De novo protein synthesis of specific factors guides oocyte maturation, progression through both meiotic divisions, and early embryogenesis (3, 4). Promoting or preventing translation is regulated by RNA-binding proteins (RBPs) (5, 6). They form messenger ribonucleoprotein complexes (mRNPs) by binding to mRNA targets, and thereby control mRNA half-lives or interactions with the core protein synthesis machinery (5, 6). Thus, the protein composition of an mRNP is a major determinant of collective mRNA activities and protein synthesis amounts.

Remodeling of an mRNP may be achieved by posttranslational modifications of its protein constituents. For instance, in mammalian cells, ubiquitination of the RBP HuR promotes its release from mRNPs, leading to the turnover of HuR target mRNAs but not HuR protein (7). In frog oocytes, phosphorylation of cytoplasmic polyadenylation element (CPE)-binding protein (CPEB) affects its interactions with other mRNP components, resulting in translational activation of CPE-containing target mRNAs (8, 9). Interestingly, hyperphosphorylation of CPEB causes its degradation and subjects its target mRNAs to further translational regulation, mediated by other RBPs (10, 11). While regulation of mRNP composition by posttranslational modifications creates an intriguing link between signaling pathways and regulated protein synthesis, the prevalence of its coupling to selective protein degradation is less clear.

In the cytosol, selective protein degradation is usually performed by the ubiquitin-proteasome system (UPS), which covalently modifies target proteins by the attachment of the polypeptide ubiquitin, converting them into substrates of the proteasome, a multisubunit protease (12). Ubiquitination is performed by target-specific ubiquitin ligases, and it is preceded by phosphorylation of the target protein in many cases (13). A requirement for protein phosphorylation before its recognition by ubiquitin ligases allows coupling the turnover of a target protein to processes that are regulated by kinases and phosphatases (14). For this reason, selective degradation plays a signaling-dependent regulatory role by reducing the abundance of its protein components (e.g., in cell cycle progression) by removing certain regulators (e.g., cyclins, cyclin-dependent kinase inhibitors) as a response to cyclin-dependent kinase activities (14). An important aspect of protein degradation in regulating developmental processes is that the turnover of a regulatory protein prevents reiteration of already executed stages. Repetition

Significance

RNA-binding proteins (RBPs) are key regulators of gene expression. Notably, germ cells deploy many distinct RBPs to guide their differentiation into haploid gametes. While the RNA-regulatory functions of RBPs are emerging, mechanisms controlling their activities and abundance are poorly understood. Due to its highly refined spatial organization, the gonad of *Caenorhabditis elegans* is an excellent model system to study temporal controls of RBP abundance. We used it to uncover a kinase-mediated protein-turnover axis that is built of evolutionarily conserved components, arranged in a unique manner, to couple RBP-target mRNA de-repression with RBP elimination at pachytene exit, a critical stage in early meiosis. This work reveals how meiotic cell cycle progression is coupled to tissue-specific differentiation events via signaling-induced RBP turnover.

Author contributions: E.K., R.M., and C.R.E. designed research; E.K. and R.M. performed research; E.K. and R.M. contributed new reagents/analytic tools; E.K., R.M., and C.R.E. analyzed data; and E.K. and C.R.E. wrote the paper.

The authors declare no conflict of interest.

This article is a PNAS Direct Submission. D.G. is a guest editor invited by the Editorial Board.

[1]To whom correspondence should be addressed. Email: christian.eckmann@genetik.uni-halle.de.

This article contains supporting information online at www.pnas.org/lookup/suppl/doi:10.1073/pnas.1715439115/-/DCSupplemental.

Published online March 1, 2018.

of a stage would require another round of the synthesis of the regulator, thereby achieving linearity of the entire process. Whereas destabilization of certain cell cycle regulators has been intensively investigated, our knowledge about UPS-mediated mRNP regulation in developmental processes is poorly understood.

In this work, we set out to elucidate the molecular mechanism of how germ cells synchronize early meiotic progression with sexual differentiation through ubiquitin-mediated degradation of RBPs. By focusing on *Caenorhabditis elegans* oogenesis, we investigated two distinct but widely conserved RBP families. We chose one representative of each (GLD-1/STAR and CPB-3/CPEB), as both protein expression patterns are restricted to early meiotic prophase (15, 16). Both RBPs encode RNA sequence-specific translational regulators that promote oogenesis (15, 17, 18). The mRNA target repertoire of the tumor suppressor GLD-1 has been especially well characterized, revealing its role as a translational repressor of mRNAs that encode factors important for oocyte meiotic progression, differentiation, and maturation, such as OMA-1 and OMA-2 (18–20). Although GLD-1 and CPB-3 share no obvious amino acid sequence similarities, we identified a shared mechanism that drives the rapid decline of GLD-1 and CPB-3 protein levels at the transition from pachytene to diplotene in meiotic prophase, before overt sexual differentiation.

We found that a polyubiquitin ligase regulates the abundance of both RBPs during gametogenesis in a stage-specific manner, similar to the degradation of cell cycle regulators. Timing of degradation is regulated by the activity of a MAPK, which integrates progression through meiosis and oocyte differentiation with signaling from neighboring somatic cells. Together, our work suggests that a developmental series of stereotyped posttranslational modifications operates in germ cells on distinct RBPs to synchronize gamete progression through meiosis and development according to sexual identity with posttranscriptional gene expression programs.

Results

The Proteasome Reduces GLD-1 and CPB-3 Levels Past Pachytene. To determine the factors that shape the expression pattern of GLD-1 and CPB-3, we investigated the abundance of these proteins during oogenesis by focusing on the prophase of meiosis I. The *C. elegans* gonad is a convenient system for studying germ cell development: All germ cells are linearly arranged in a spatiotemporal gradient of maturation, extending from the distal end to the proximal end of the gonad (21). The developmental stage of a cell is approximated by its position relative to its neighbors within the gonad, and is determined more precisely by the nuclear appearance of its chromatin organization, visualized with DNA stains (Fig. 1*A*). Due to this reproducible organization with high temporal resolution, immunofluorescent microscopy images of extruded gonads stained for endogenous GLD-1 and CPB-3 protein levels reveal a similar expression profile throughout oogenesis (Fig. 1 *B* and *D*).

To test whether the UPS is important for regulating the abundance of GLD-1 and CPB-3 during the meiotic prophase of oogenesis, we reduced the activity of the proteasome by RNAi-mediated depletion of *pbs-6*, which encodes one of the catalytic subunits residing in the proteasome core (22). After 36 h of exposure to RNAi, we immunostained extruded gonads and compared them with controls. Superficially, GLD-1 accumulated to similar levels in leptotene, zygotene, and pachytene cells of *pbs-6*–depleted and control animals (Fig. 1 *B* and *C*). However, compared with controls, GLD-1 levels did not immediately decrease at the pachytene-to-diplotene transition and started to tamper off in diplotene cells until GLD-1 signals were lost in diakinetic oocytes of *pbs-6* RNAi-treated animals (Fig. 1 *B* and *C*). To exclude the possibility that the observed change in GLD-1 expression pattern is a fixation or permeabilization artifact, we performed *pbs-6* RNAi in a transgenic strain that expresses GLD-1::GFP and analyzed protein distribution in anesthetized animals. The GLD-1::GFP expression pattern recapitulates that of the endogenous protein in control conditions (Fig. S1*A*), and GLD-1::GFP levels extend further into diplotene cells upon partial *pbs-6* reduction (Fig. S1 *B* and *D*). These observations suggest that proteasome activity contributes to the rapid decrease of GLD-1 at the pachytene-to-diplotene transition, but not to its complete clearance in diakinetic oocytes.

We observed a similar impact of *pbs-6* RNAi on the expression pattern of CPB-3. While no obvious change was visible before pachytene exit, cells at the pachytene-to-diplotene transition and in diplotene contained higher levels of CPB-3 upon proteasome inhibition relative to its control counterparts (Fig. 1 *D* and *E*). To quantify observed changes, we measured the intensity of anti–CPB-3 signal 100 μm distally and proximally from the pachytene-to-diplotene border, which was determined by DAPI-stained chromatin morphology across the entire depth of the gonad (Fig. 1*F*). The *pbs-6* RNAi led to an extension of CPB-3 signals beyond pachytene exit, and the reduction of CPB-3 levels was delayed compared with controls (Fig. 1*F*), suggesting that proteasome activity restricts CPB-3 expression pattern in post-pachytene female germ cells.

Our observations suggest that the UPS reduces both RBPs at the pachytene-to-diplotene transition, potentially via a common pathway. However, other combined roles of the proteasome in regulating both GLD-1 and CPB-3 are possible, although our limited RNAi knockdown regime may preclude us from discovering such roles. Consistent with this limitation, we did not detect overt changes in the total levels of either germ-cell–specific RBP by analyzing worm extracts of partially *pbs-6*–depleted and control animals by Western blotting (Fig. S1*E*). Moreover, as GLD-1 and CPB-3 levels are eventually decreased in fully differentiated oocytes (Fig. 1 *C* and *E* and Fig. S1*B*), other proteasome, or even nonproteasomal, mechanisms may exist in maturing oocytes to clear out these RBPs.

***Sel-10* Removes both RBPs in Postpachytene Oocytes.** To identify a ubiquitin ligase that destabilizes GLD-1 and CPB-3, we performed a Y2H screen. In contrast to GLD-1, full-length CPB-3 fusions were expressed well and gave reproducible results. Thus, we used CPB-3 as bait in search for interacting proteins and identified 396 positive clones: 54 contained fragments of *sel-10* ORF. The *sel-10* encodes an F-box and WD40 repeat (FBXW) protein homologous to the human tumor suppressor FBXW7. FBXW proteins have been described in various systems, including *C. elegans*, to serve as substrate recognition components of the SCF class of E3 ubiquitin ligases (23, 24). Hence, SEL-10 was a promising candidate for a determinant of CPB-3 stability.

Whereas F-box domains bind to Skp1-related adapter proteins of SCF complexes, WD40 domains recognize SCF target proteins (24). Consistent with this general notion, SEL-10 lacking the F-box domain (SEL-10ΔF) did not interact with the Skp1-related adapter protein of SCF complexes, SKR-1 (25) (Fig. 2*A*). However, SEL-10ΔF was able to interact with CPB-3 (Fig. 2*A*), which is also consistent with the recovered clones in the Y2H screen as all contained the WD40 domain in full. Moreover, SEL-10ΔF::DB and GLD-1::AD coexpressing clones reproducibly turned blue in β-galactosidase assays, indicating a likely interaction between the two-hybrid proteins (Fig. 2*A*). Lastly, upon coexpression of epitope-tagged SEL-10 fragments with CPB-3 in insect cells followed by immunoprecipitation analysis, we observed a much stronger enrichment of the WD40-containing C terminus over the F-box–containing N terminus (Fig. S2 *C* and *D*). Thus, SEL-10 may directly interact with both RBPs primarily via its WD40 repeats.

To test whether SEL-10 restricts germ cell expression of GLD-1 and CPB-3, we analyzed immunostained extruded gonads of the likely null mutant animals *sel-10(ok1632)* [henceforth referred to as *sel-10(0)* (25)]. Similar to the effect observed upon *pbs-6* RNAi, a lack of *sel-10* activity resulted in elevated levels of GLD-1 at pachytene exit compared with controls (Fig. 2 *B* and *C*). Furthermore,

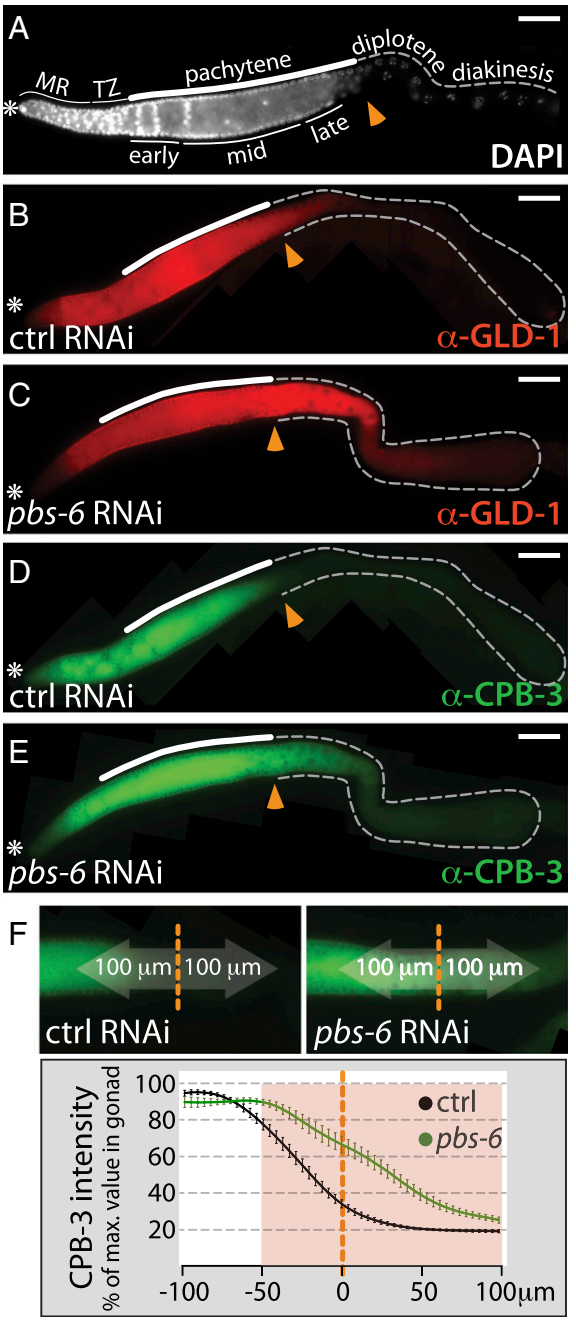

Fig. 1. Proteasome activity shapes GLD-1 and CPB-3 expression patterns in the germ line. (*A–E*) Germ cell organization of extruded hermaphroditic gonads. An asterisk indicates the distal end, a white thick line indicates the pachytene region, a gray dashed outline indicates the proximal part of the gonad, and an orange arrowhead indicates the pachytene-to-diplotene border. (Scale bars: 50 µm.) (*A*) DAPI staining reveals meiotic stages. The most distal end of the gonad is referred to as the mitotic region (MR), and contains proliferating germ-line stem cells and cells in premeiotic S-phase. The further proximally located transition zone (TZ) harbors cells in the first two stages of meiotic prophase, leptotene and zygotene, revealing a crescent-shaped chromatin organization. Pachytene nuclei occupy the rest of the distal part of the gonad, nearly until the bend region. Shortly before the bend region, cells transit to diplotene, which transition is demonstrated by partial relaxation of chromatin and initiation of oocyte growth. Oocytes arrested in diakinesis reside in the proximal part of the gonad. (*B–E*) Anti–GLD-1 and anti–CPB-3 immunostaining shows altered expression patterns upon proteasome inhibition by *pbs-6* RNAi. (*F*) Measurements of immunofluorescent signal intensity around the pachytene-to-diplotene border (dashed line). (*Top*) Scheme of analyzed region. (*Bottom*) Typical decrease of CPB-3 levels after pachytene exit is delayed upon proteasome inhibition. Error bars show SEM ($n = 10$ gonads of each genotype), and the pink-shaded region indicates signal intensity differences of statistical significance (*t* test: $P < 0.05$). max., maximum.

GLD-1 was clearly detectable in the proximal part of the gonad, with a stepwise decrease in signal intensity until the last oocyte (Fig. 2 *B* and *C*). Also, CPB-3 levels remained high at the pachytene-to-diplotene transition and in diplotene cells of *sel-10(0)* gonads (Fig. 2 *D* and *E*). Although the extension of its expression pattern was less pronounced compared with GLD-1, a quantification of anti–CPB-3 signals around the P-D border indicated a significant difference between *sel-10(0)* and wild-type gonads (Fig. S2 *A* and *B*). Moreover, a similar extension of CPB-3 and GLD-1 levels was observed upon RNAi-mediated knockdown of the homolog of Cullin1, *cul-1*, which encodes the central scaffold protein of SCF ubiquitin ligases (24) (Fig. S2 *A* and *B*). Together, these observations suggest that during meiosis, *sel-10* regulates GLD-1 and CPB-3 abundance, most likely operating as an SCF complex component.

SEL-10 Acts Posttranslationally. While GLD-1 expression is turned on by posttranscriptional control (i.e., translational control) (26, 27), we find that GLD-1 is posttranslationally turned off. To provide further evidence that *sel-10* destabilizes GLD-1 protein rather than controlling its translation, we analyzed the distribution of a LAP-tagged GLD-1 fusion protein that is produced from ubiquitously expressed mRNAs containing either unregulated beta-tubulin-2 (*tbb-2*) or translationally repressed *gld-1* 3′UTR sequences (Fig. 2 *F* and *G*). Consistent with previous results (20, 27), we observed a uniform distribution of GLD-1::LAP(*tbb-2 3′ UTR*) in the distal part of the gonad: Mitotically dividing and early meiotic cells until mid- to late pachytene produced similar protein amounts (Fig. 2 *F* and *G*), while GLD-1::LAP(*gld-1 3′UTR*) levels stayed low in premeiotic cells. This is consistent with up-regulation of GLD-1 via translational control. Importantly, in the proximal part of the gonad, GLD-1::LAP levels were reduced and similarly low when produced from either 3′UTR-containing mRNA (Fig. 2 *F* and *G*). This argues that in postpachytene cells, GLD-1 abundance is regulated at the posttranslational level.

To test whether a reduction of GLD-1::LAP levels is mediated by SEL-10, we knocked down *sel-10* activity by RNAi feeding and analyzed fluorescent protein levels in anesthetized animals. In contrast to controls, *sel-10* depletion elevated proximal levels of GLD-1::LAP(*gld-1 3′UTR*) (Fig. 2 *F* and *G*), recapitulating results obtained for GLD-1::GFP and endogenous GLD-1 (Fig. S1 *A–C*). Importantly, *sel-10* depletion also increased proximal levels of GLD-1::LAP(*tbb-2* 3′UTR) to similar levels of GLD-1::LAP(*gld-1 3′UTR*) (Fig. 2 *F* and *G*), suggesting that *sel-10* regulates GLD-1::LAP by recognizing the amino acid sequence rather than 3′UTR sequences regulating mRNA translation.

As we did not observe any effect on the expression of either RBP in distal parts of *sel-10*–deprived gonads (Fig. 2*F*), *sel-10* likely acts in later prophase to decrease GLD-1 and CPB-3 abundance before oogenesis completion, arguing that *sel-10* activity might be restricted to late pachytene/postpachytene stages. Knowing that *sel-10* mRNA is uniformly present in the adult gonad (Nematode Expression Pattern DataBase), we analyzed the chromatin-localized translational reporter GFP::histone 2B(*sel-10* 3′UTR) and found that its nuclear fluorescence was weak in premeiotic and early prophase cells. However, reporter expression increased in mid- to late pachytene, and persisted past pachytene although at lower levels (Fig. S2*F*). These data suggest that SEL-10 is generally expressed in proliferative and meiotic cells but accumulates in midpachytene, just before its

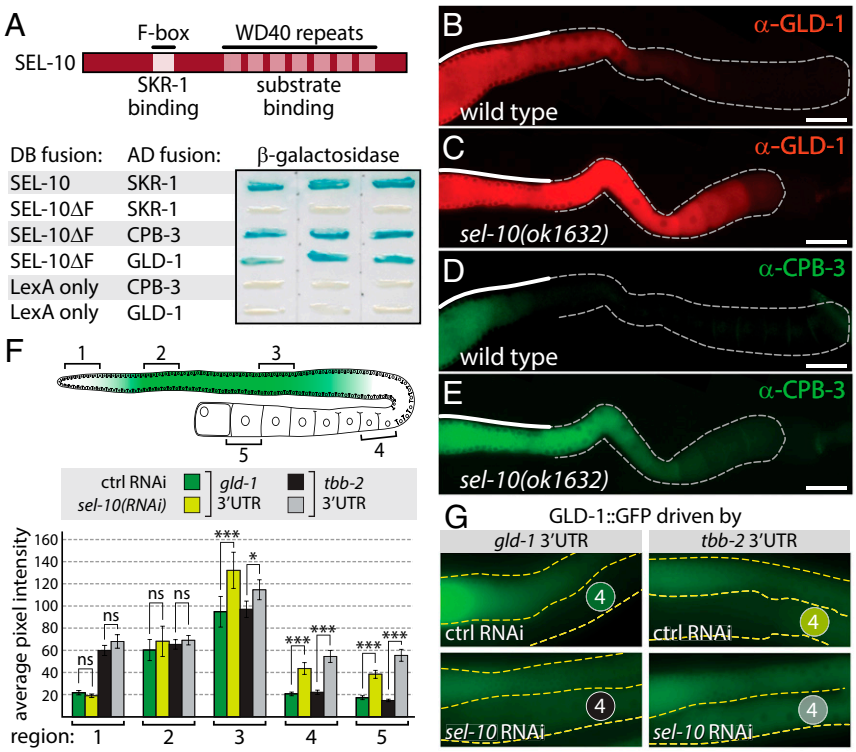

Fig. 2. SEL-10 regulates GLD-1 and CPB-3 levels. (*A*) SEL-10 interacts with CPB-3 and GLD-1 in a Y2H assay. The F-box protein adapter SKR-1 binds to SEL-10 in an F-box–dependent manner, while CPB-3 and GLD-1 bind to SEL-10 in an F-box–independent manner. (*B–E*) Immunofluorescent staining shows extended expression of GLD-1 and CPB-3 during meiosis in *sel-10(0)* mutants. (Scale bars: 50 μm.) (*F*) Quantification of the intensity of GLD-1::LAP fluorescence. Five gonadal regions of GLD-1::LAP intensity measurements are indicated. Loss of *sel-10* stabilizes GLD-1::LAP levels in the proximal gonad independent of the 3′UTR used to direct fusion-protein expression. Error bars show SD ($n = 10$ gonads of each genotype) (*t* test: $^*P < 0.05$ and $^{***}P < 0.001$). ns, not significant. (*G*) Fluorescence in the germ lines of anesthetized control RNAi or *sel-10*–depleted animals expressing GLD-1::LAP under the control of *gld-1* or *tbb-2* 3′UTRs. The indicated region 4 corresponds to the data summarized in *F*.

presumed role in RBP turnover. Taking all data together, we propose that SEL-10 functions as a substrate recognition subunit of an $SCF^{SEL\text{-}10}$ complex that mediates ubiquitination and destabilization of GLD-1 and CPB-3 in postpachytene oocytes.

Phosphorylation Is Likely to Precede Ubiquitination of both RBPs. Substrate recognition by F-box proteins usually depends on prior phosphorylation of target proteins (14). Thus, in the absence of the specific ubiquitin ligase, phosphorylated protein forms may accumulate. To test whether both RBPs are phosphorylated before their degradation, we analyzed worm protein extracts by immunoblotting (Fig. 3). Whereas CPB-3 migrated as a single band in wild type, multiple slower migrating bands were observed in *sel-10(0)* (Fig. 3 *A* and *B*). Similar data were obtained for GLD-1 (Fig. 3*D* and Fig. S3*A*). To confirm that the additional bands represent phosphorylated RBPs, we treated the *sel-10(0)* extract with λPP. Preparing the extract suitable for this assay was difficult as modified forms of CPB-3 were very unstable, even when high concentrations of several phosphatase inhibitors were used. We overcame these difficulties by precipitating proteins from crushed worms with TCA before resuspending the precipitated material in a λPP buffer. Incubation of the extract with the phosphatase removed slow-migrating forms of CPB-3 (Fig. 3*A*), indicating that these additional bands represent phosphorylated CPB-3, and suggests that hyperphosphorylation may precede CPB-3 degradation.

To find out whether CPB-3 phosphorylation is unique to *sel-10(0)* mutants or occurs also in wild type, we attempted to detect modified CPB-3 forms in wild-type extracts using Phos-Tag gel electrophoresis, which retards phosphorylated proteins (28). At least three differently migrating CPB-3 forms were distinguishable (Fig. S3*B*), which are sensitive to λPP treatment (Fig. S3*C*). Although we could not resolve TCA-precipitated wild-type extracts as finely as *sel-10* extracts on Laemmli gels (Fig. 3*A*), λPP treatment increased CPB-3 mobility in the Phos-Tag gel (Fig. S3*C*), indicating that the smearing behavior of nontreated samples stems from the presence of phosphorylated CPB-3. Therefore, CPB-3 is also phosphorylated in wild type, but hyperphosphorylated CPB-3 is difficult to detect at steady state. By contrast, GLD-1 hyperphosphorylation is more readily visible in standard gel electrophoresis (Fig. S3*A*), which may simply reflect a difference in individual RBP abundance. Importantly, we observed that slower migrating CPB-3 and GLD-1 forms accumulate upon RNAi knockdown of *cul-1*, but not of *cul-2* or *cul-3* (Fig. S3*D*), suggesting that the accumulation of phospho–GLD-1 and phospho–CPB-3 is specifically linked to the reduced activity of the $SCF^{SEL\text{-}10}$ ubiquitin ligase. Moreover, an accumulation of both phospho-RBP forms is not observed upon reduction of the β-TrCP homolog of SEL-10, LIN-23/FBXW1 (Fig. S3 *E* and *F*), which is also consistent with its inability to bind CPB-3 in yeast (Fig. S2*E*). We conclude that phosphorylated forms of GLD-1 and CPB-3 accumulate in the absence of $SCF^{SEL\text{-}10}$ activity and that destabilization of both RBPs is likely regulated by phosphorylation.

MPK-1 Affects the Phosphorylation Status and Abundance of both RBPs. To reveal which kinase regulates the stability of GLD-1 and CPB-3, we tested several candidates. Whereas relatively little is known about regulation of STAR protein stability, regulation of CPEB degradation has been investigated in various organisms (29–31). In frog oocytes, the degradation is triggered by consecutive phosphorylation of CPEB1 by a cyclin-dependent kinase, Cdk1, and a polo-like kinase, Plx1 (32). Hence, we performed RNAi against the

DEVELOPMENTAL BIOLOGY

corresponding genes, *cdk-1* and *plk-1*. Despite efficient gene knockdown, judged by 100% penetrant embryonic lethality and nuclear aberrations of mitotically dividing cells in the distal gonad, we did not observe any extension of the CPB-3 expression pattern in postpachytene cells (Fig. S3*G*), arguing that neither CDK-1 nor PLK-1 is required to destabilize CPB-3.

The *C. elegans* MAPK, MPK-1, is essential for meiotic progression and regulates multiple other processes during oogenesis (33, 34). As MPK-1 is active in mid- to late pachytene and diakinetic oocytes (33, 34), we tested whether it influences GLD-1 and CPB-3 levels. As a complete lack of MPK-1 activity in *mpk-1(0)* mutants results in no postpachytene cells (35), we reduced *mpk-1* activity only partially by mild RNAi knockdown. Although those gonads displayed weak *mpk-1(0)*–like phenotypes, they maintained a typical female gonadal organization overall and contained postpachytene cells. In these *mpk-1(RNAi)* animals, CPB-3 (Fig. S3*G*) expression was prolonged into late pachytene and postpachytene cells, suggesting that MPK-1 functions in regulating CPB-3 and, presumably GLD-1, stability.

To strengthen these results, we tested whether a reduction of *mpk-1* activity affects accumulation of both phosphorylated RBPs. As the phosphorylation status of CPB-3 is best surveyed in *sel-10(0)* animals, we performed our Western blot analysis in this mutant background. Significantly lower amounts of modified CPB-3 were detected in *mpk-1*–depleted than control animals (Fig. 3 *B* and *C*), demonstrating that MPK-1 affects the phosphorylation status of CPB-3. Unexpectedly, we also observed in *sel-10(0)* animals an increase in total amounts of CPB-3 upon partial *mpk-1* RNAi (Fig. 3 *B* and *C*). This additive effect may point at a SEL-10–independent mechanism to down-regulate CPB-3 or, alternatively, may be indirect and a consequence of disorganized germ cells in MPK-1–depleted gonads. Importantly, similar observations were made for GLD-1 phosphorylation and abundance (Fig. 3 *D* and *E*), arguing that MPK-1 regulates the phosphorylation status, and thereby protein stability, of either RBP.

Next, we asked whether MPK-1 phosphorylates GLD-1 and CPB-3 directly or, instead, exerts its action via downstream kinases. To test whether MPK-1 binds to GLD-1 and CPB-3, we performed Y2H assays. As a positive control for the interaction, we used NOS-3, an RBP that is a known MPK-1 target (36). MPK-1::AD interacted with GLD-1::DB and CPB-3::DB hybrids as it did with NOS-3::DB (Fig. 3*F*). Thus, MPK-1 might directly bind and modify GLD-1 and CPB-3, and serve as a regulator of their stability in germ cells.

Prolonged Expression and Hyperphosphorylation of GLD-1 May Affect Its Translational Activity. Extended expression of GLD-1 and CPB-3 may lead to timing defects of target mRNA translation. Due to the lack of established target mRNAs of CPB-3, we investigated this possibility by focusing on GLD-1, and asked whether its prolonged expression in postpachytene cells may interfere with a timely translational de-repression of target mRNAs. We chose to focus on two well-established oocyte maturation proteins and analyzed the accumulation of OMA-1 and OMA-2 (37), which are detected here with a pan-antibody and collectively referred to as OMA. In immunostained wild-type gonads, OMA is not detectable in the distal part of the gonads, but it starts accumulating at the bend region in postpachytene cells and gradually enriches during diakinesis, resulting in a complimentary expression pattern to GLD-1 (Fig. 4*A*). In *sel-10(0)* gonads, GLD-1 levels remained relatively high at the bend region and the accumulation of OMA appeared delayed (Fig. 4*A*). Interestingly, our quantification of signal intensities revealed that OMA began accumulating in *sel-10(0)* at the same time as in wild type but that its expression remained lower for four to five oocyte widths (Fig. 4*B*). OMA expression then became similar ~200 μm proximal from the pachytene-to-diplotene border. We conclude that the prolonged expression of GLD-1 has a negative, although limited, impact on efficient translation of its mRNA targets. This suggests that further mechanisms, as yet unknown, may contribute to a postulated translational de-repression of GLD-1 target mRNAs upon GLD-1 reduction (18).

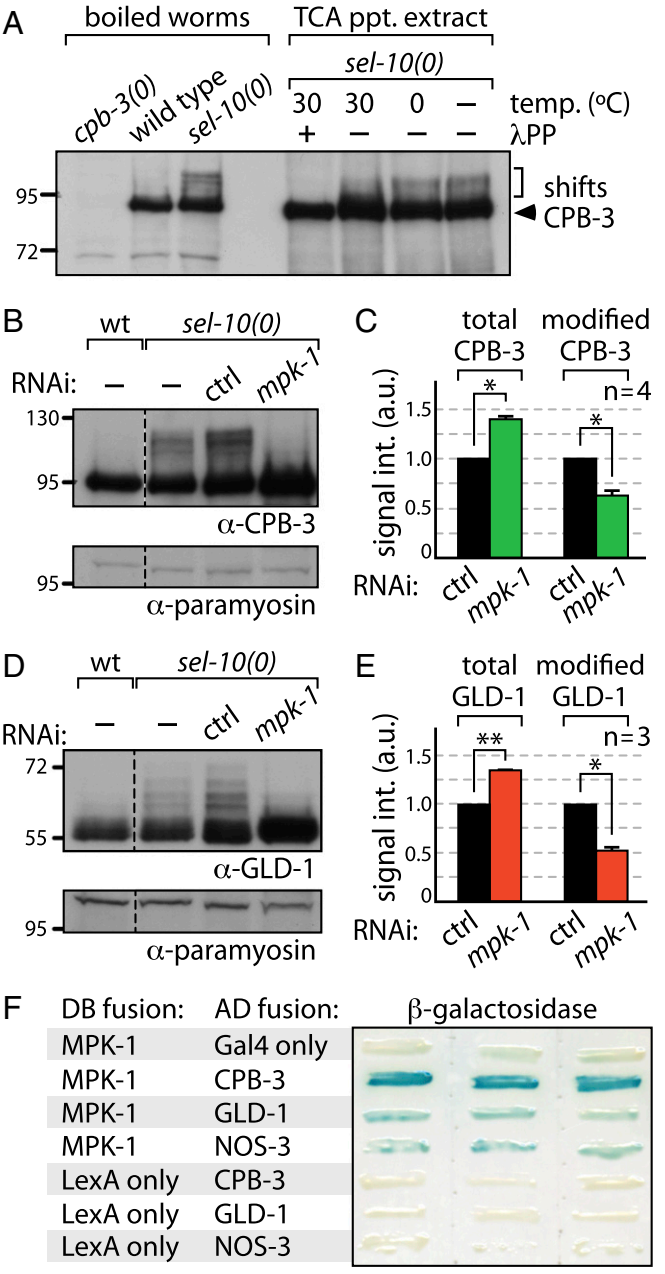

Fig. 3. MPK-1 regulates phosphorylation status and abundance of GLD-1 and CPB-3. (*A*) Phosphorylated forms of CPB-3 accumulate in *sel-10(0)* mutant worms, as shown by Western blotting. Modified CPB-3 forms are sensitive to λPP treatment. The last lane contains an aliquot of the same TCA-precipitated extract that was immediately boiled in sample buffer without additional treatment. Two biological repetitions of TCA-precipitated extracts were analyzed with similar results. Loading: 50 worms each in the first three lanes. ppt, precipitated; temp., temperature. The accumulation of phosphorylated CPB-3 (*B* and *C*) and GLD-1 (*D* and *E*) in *sel-10(0)* worms depends on *mpk-1* activity. (*B* and *D*) Western blotting analysis of worm extracts. Dashed lines indicate where parts of the blot were removed for clarity. wt, wild type. (*C* and *E*) Quantitation of the signal coming from total and modified protein forms (*t* test: $*P < 0.05$ and $**P < 0.01$). (*F*) MPK-1 interacts with CPB-3 and GLD-1 in a Y2H assay. None of the hybrid proteins used in the study was able to trigger expression of the reporter gene when coexpressed with a non-hybrid DNA-binding (LexA only) or AD (Gal4 only) fusion protein.

One possible mechanism might be that GLD-1 in postpachytene oocytes of *sel-10(0)* worms is hyperphosphorylated and represses translation inefficiently in this form. To investigate whether the phosphorylation status of GLD-1 correlates with the stage of meiosis, we compared the phosphorylation status of tagged GLD-1 (GLD-1::LAP) in pachytene and postpachytene cells. To express GLD-1::LAP exclusively in postpachytene cells, we used the 3′UTR of *oma-2* mRNA and detected the fusion protein only in the proximal part of the gonad, albeit at much lower levels than GLD-1::LAP(*gld-1* 3′UTR) in the pachytene region of wild-type animals (Fig. S4*A*). Importantly, *sel-10* RNAi increased the levels of GLD-1::LAP(*oma-2* 3′UTR) but, otherwise, did not influence its expression pattern (Fig. S4*A*), arguing that SEL-10 is continuously active in postpachytene cells. As is the case for the endogenous GLD-1 protein (Fig. 3*D*), numerous forms of GLD-1::LAP(*gld-1* 3′UTR) were detected: a fast migrating unmodified form, a predominant form of slower migration, and multiple additional upshifting forms, which are all proportionally more pronounced in *sel-10* than in control RNAi (Fig. S4*B*). However, when GLD-1::LAP was expressed from *oma-2* 3′UTR, no predominant band was observed and the upshifting bands appeared equal in intensity, suggesting that a majority of hyperphosphorylated forms are now present in oocytes. This effect was even more pronounced upon *sel-10* RNAi, in which the slower migrating forms of GLD-1::LAP were as abundant as in GLD-1::LAP(*gld-1* 3′UTR)-expressing worms, but the predominant faster migrating form was missing (Fig. S4*B*). We conclude that GLD-1 is more likely to be phosphorylated in the proximal, oogenic part of the gonad than in the distal, predominantly pachytene part of the gonad, which is also consistent with the subsequent strong activity of MPK-1 in maturing oocytes (33, 34). We propose that this phosphorylation may have an influence on the repressive activity of GLD-1.

Discussion

This work reports the synchronized degradation of two distinct RBPs during meiotic prophase, which is mediated, in part, by the SCF^{SEL-10} ubiquitin ligase. Correlated with pachytene exit, we find that MAPK signaling activity leads to hyperphosphorylation of both RBPs, flagging both proteins for F-box–mediated target recognition (Fig. 4*C*). Although neither translational regulator was identified in previous bioinformatic screens for SEL-10 and MPK-1 targets (33, 38), we demonstrate that SEL-10/FBXW7 and MPK-1/MAPK bind to CPB-3/CPEB and GLD-1/STAR in heterologous systems. Hence, we propose that MAPK and FBXW7 form a regulatory pathway in germ cells to coordinate meiotic progression with posttranscriptional gene expression programs of gametogenesis.

Translational Control Combined with Posttranslational Regulation Shapes RBP Expression Dynamics. Translational control plays a prevalent role in regulating gametogenesis, stressing the need to understand how the abundance and activity of RNA regulators are regulated during germ cell development. Not surprisingly, numerous examples of different RBP families across phyla suggest that RBPs are themselves subject to posttranscriptional regulation, mediated by *cis*-elements located in their cognate mRNAs (39–41). Also, likely auto-regulatory feedback loops have been proposed for numerous RBPs, such as fly Oskar (42), frog Dead end1 (43), mammalian DAZAP1 (44), and worm PUF (45, 46) proteins. Also, the expression patterns of GLD-1 and CPB-3 are likely shaped by regulated translation, as indicated by the expression patterns of 3′UTR translational reporters (27). Moreover, GLD-1 has been found to associate with its own mRNA (19, 20), and the *cpb-3* mRNA contains several potential CPEB-binding sites. However, the details of these posttranscriptional mechanisms are still unknown.

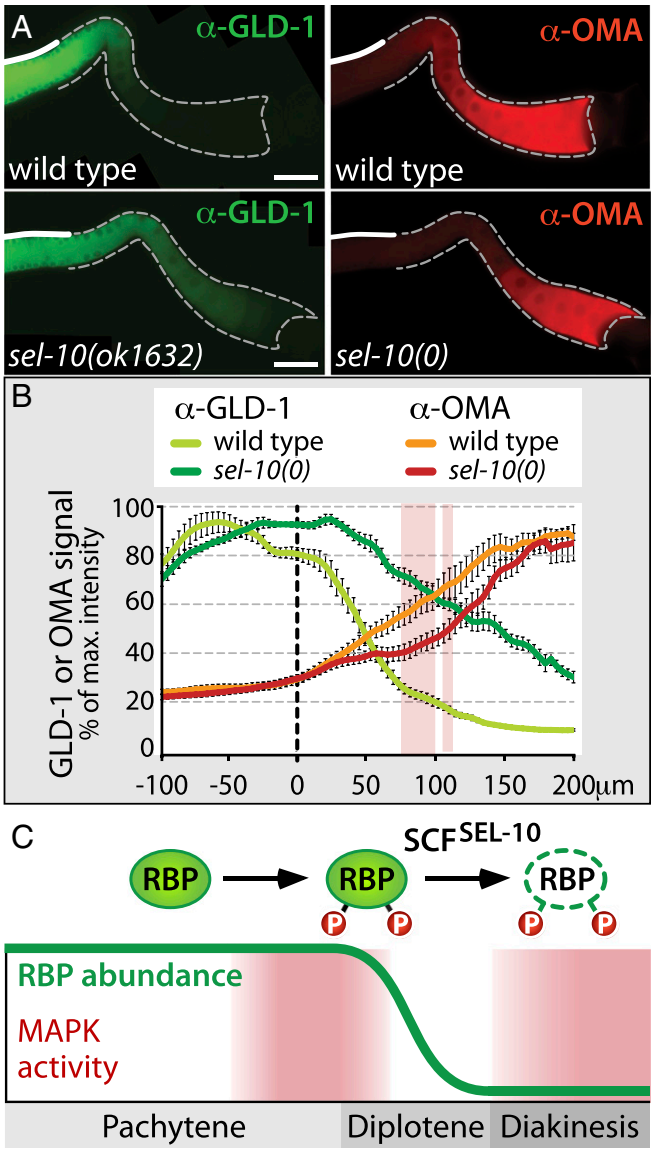

Fig. 4. Prolonged expression of GLD-1 impacts target mRNA translation. (*A*) Immunostaining showing extended GLD-1 expression and delayed OMA accumulation in *sel-10(0)* germ lines. (Scale bars: 50 μm.) (*B*) Quantification of the immunosignal at the indicated distance from the pachytene-to-diplotene transition (represented by the dashed *y* axis). Error bars indicate SEM, and the pink-shaded region indicates OMA signal intensity differences of statistical significance (*t* test: $P < 0.05$; $n = 6$). max., maximum. (*C*) Model of MPK-1–controlled and SCF^{SEL-10}–mediated degradation of the two RBPs, CPB-3 and GLD-1, during *C. elegans* oogenesis (relevant meiotic stages on the *x* axis). MPK-1 has two activity maxima during oogenesis (red-shaded areas).

In postpachytene cells, the expression patterns of 3′UTR translational reporters are extended in comparison to the endogenous protein patterns (26), suggesting that additional posttranslational mechanisms are at play to restrict the abundance of CPB-3 and GLD-1 proteins during oogenesis. Here, we find that CPB-3 and GLD-1 undergo regulated degradation by the UPS. Thus, at least two independent mechanisms operate in meiotic germ cells to restrict the levels of these two conserved RBP families, and to limit their impact on the gene expression program during gametogenesis.

MAP Kinase Is a Central Regulatory Factor of Gametogenesis. Reduction of both translational regulators is synchronized with

DEVELOPMENTAL BIOLOGY

meiotic progression through the activity of the MAPK signaling pathway. Across phyla, MAPK is an important regulator of oocyte meiotic resumption, essential for the consecutive completion of both meiotic divisions: (*i*) MAPK controls the activity of upstream kinases and phosphatases that converge on the maturation-promoting factor (MPF), which is a heterodimer of CDK-1 and cyclin B (47); (*ii*) it stimulates protein synthesis of factors that promote meiotic progression, such as cyclin B (48, 49); and (*iii*) it positively or negatively influences the stability of other regulatory proteins (50, 51). Importantly, it has recently been shown that a MAPK cascade triggers the degradation of CPEB1 to promote meiotic progression in mice (49). MAPK was also found to phosphorylate CPEB before meiotic resumption in clams and frogs; however, those phosphorylations were not causally linked as instructive to regulate CPEB stability (48, 52). Together with our findings in *C. elegans*, MAPK-mediated targeted destruction of CPEBs might be a universal mechanism in CPEB protein family regulation.

Contrary to CPEBs, a role of MAPK signaling in regulating the stability of STAR proteins has not been documented so far. However, MAPK-mediated activity regulation of STAR proteins is well established (53). Phosphorylation of the splicing factor and the STAR protein, Sam68, by MAPK/ERK influences alternative splicing of CD44, which is an important regulatory mechanism during embryogenesis, tumorigenesis, and immune responses in mammals (54). Also, ERK-mediated phosphorylation of Sam68 plays a role in male gametogenesis, causing its cytoplasmic relocalization to promote the expression of its mRNA targets (55). Whether MPK-1–mediated phosphorylation affects GLD-1 in its activity as a translational repressor before triggering its degradation remains to be shown. However, our work opens up the possibility that MAPK-mediated phosphorylation of STAR proteins may be an ancient regulatory module to couple STAR protein turnover with activity changes, therefore highlighting further molecular parallels between the these two distinct RBP families.

In addition to meiotic maturation, MAPK activity is important at earlier stages during *C. elegans* oogenesis (Fig. 4*C*). It is required for timely progression from mid- to late pachytene in meiotic prophase I (34) and for proper membrane organization during oocyte formation (36). Consistent with the prominent role of RNA-regulatory proteins in germ cell development, RBPs are enriched in the list of computationally identified targets of MPK-1 (34). A proven example is the translational repressor and *C. elegans* Nanos ortholog, NOS-3 (36). However, contrary to GLD-1 and CPB-3 regulation, only the RNA-binding activity of NOS-3 is inactivated upon phosphorylation by MPK-1 (36); no role in turnover has been demonstrated. As MPK-1 has not surfaced yet as a major factor regulating the stability of germ-line proteins, our work reveals a unique function of MAPK signaling during oogenesis and expands the list of known RNA regulators as MAPK/ERK targets.

RBP Turnover and Female Gametogenesis Are Regulated by Specific E3 Ubiquitin Ligase Complexes. We identified the Cullin1-based $SCF^{SEL\text{-}10}$ complex as an E3 ubiquitin ligase that controls RBP abundance in germ cells (Fig. 4*C*). Its target recognition subunit, SEL-10, is homologous to mammalian FBXW7, a known negative regulator of Notch, cyclin E, and the two protooncogenes c-Myc and c-Jun among others (23). In mice, Fbxw7 is an essential gene and genetic deficiencies cause developmental defects that lead to embryonic lethality (56). By contrast, *sel-10* is not essential in *C. elegans*, suggesting either genetic redundancy or a changed target repertoire. To date, SEL-10 is primarily known for its somatic functions: In sex determination, SEL-10 targets two FEM proteins for degradation (57); during vulva formation, SEL-10 regulates the Notch receptor LIN-12 and LIN-45/Braf, a MAPK signaling pathway component (38, 58); in neurons, SEL-10 destabilizes yet unidentified targets to regulate synapse formation during vulva innervation (59); and in the early embryo, SEL-10 reduces the activity of the cell cycle kinase ZYG-1/Plk4 to antagonize centrosome duplication (60). While a spermatogenic role of SEL-10 has recently been proposed (60), our work demonstrates a molecular role of FBXW7 proteins during female gametogenesis and expands their target repertoire to RBPs.

A number of proteins are regulated by more than one ubiquitin ligase, and our work suggests that additional turnover pathways may operate redundantly with the MAPK–SEL-10 axis to destabilize RBPs. For instance, during fly eye development, Cullin1- and Cullin3-based complexes independently act to trigger degradation of the transcription factor *Cubitus interruptus* (61). During frog oocyte maturation, the two ubiquitin ligases $SCF^{\beta\text{-}TrCP}$ and Siah1 act sequentially to regulate the CDK activator RINGO/Speedy (62). Furthermore, at least three E3 ligases, $SCF^{\beta\text{-}TrCP}$, SCF^{FBXW7}, and MULE, destabilize the mammalian prosurvival protein of the Bcl-2 family, Mcl1 (63–66). Lastly, non–Cullin-based but ubiquitin-dependent mechanisms might also contribute to proteostasis of RBPs in maturing oocytes (67).

SCF Ubiquitin Ligases May Universally Coordinate Meiosis with Sexual Differentiation. The conserved WD40 F-box protein β-TrCP/LIN-23/FBXW1 stands out as an important regulator of germ cell development in vertebrates. In addition to its role in mouse spermatogenesis, where it destabilizes the transcriptional regulator Snail1 to regulate cell adhesion, β-TrCP assumes an important role in mouse and frog oogenesis, destabilizing the mRNA regulator CPEB1 (32, 49). Intriguingly, LIN-23 and SEL-10 function cooperatively during early *C. elegans* embryogenesis (60), arguing that these structurally similar F-box proteins may generally form a functional redundant pair of E3 ubiquitin ligases. However, we found no evidence for a role of LIN-23 in restricting meiotic expression of the two RBPs GLD-1/STAR and CPB-3/CPEB. Furthermore, knockdown of *cul-1*/Cullin1 in *sel-10(0)* worms did not increase RBP abundance any further, suggesting that a likely alternative degradation pathway does not employ another SCF complex. Whether FBXW1 is the only factor destabilizing CPEBs in vertebrates, as well as whether FBXW7 also acts during mammalian germ-line development, remains to be determined.

Cell cycle-coupled turnover of RBPs during gametogenesis may be an ancient evolutionary mechanism to synchronize meiotic progression with germ cell differentiation programs. Specifically, MAPK and SCFs may form a regulatory axis that is conserved among vertebrates and invertebrates. However, *C. elegans* and vertebrates utilize different F-box proteins to trigger CPEB degradation. Interestingly, this apparent contrast between species highlights intrinsic developmental timing differences of CPEB protein removal and may reflect on different CPEB activity needs. In *C. elegans*, CPB-3 degradation takes place in undifferentiated germ cells during meiotic prophase: at the transition from pachytene to diplotene. In vertebrates, CPEB degradation occurs later: during meiotic maturation, the stage that prepares fully grown female germ cells to leave meiotic prophase and enter the first meiotic division (68). Thus, likely roles of CPB-3 might resemble those of early meiotic activities of CPEBs in clam, frog, and mouse oocytes, where they act as translational repressors (52, 69, 70). Later developmental roles of CPEBs in translationally regulating the two consecutive nuclear divisions in female meiosis might have been replaced in worms by other RBPs. In analogy to CPEBs, a coupled phosphorylation/degradation mechanism may control the activity of STAR proteins. During early female meiosis of *C. elegans*, GLD-1 prevents the precocious synthesis of oocyte-specific proteins (18–20, 71). Hence, a phosphorylation-dependent switch from translational repression to de-repression may release GLD-1 mRNA targets. The coupled $SCF^{SEL\text{-}10}$-mediated

turnover of GLD-1 at pachytene exit enforces this switch, ensuring its irreversibility.

In many diverse species, pachytene marks a critical stage in gametogenesis: Homologous chromosomes are prepared for the two chromosome segregation phases, and germ cells start to differentiate according to their sexual identity using defined gene expression programs (4, 72). Therefore, it is possible that known chromosomal checkpoints operating at pachytene exit may also signal a simultaneous removal of diverse RBPs via a MAPK-SCF axis to orchestrate meiotic progression with differentiation.

Materials and Methods

Strains. *C. elegans* strains were handled according to standard procedures (73). Worms were grown at 20 °C on nematode growth media plates seeded with OP50 bacteria and typically analyzed at an age of 36 h past mid-larval stage (L)4. We obtained the presumed null alleles *sel-10(ok1632)* (25) from the *Caenorhabditis* Genetics Center (CGC) and *cpb-3(tm1746)* (15) from the Japanese Deletion Mutant Consortium, and outcrossed them 10 times with the wild-type strain Bristol N2. The null allele *sel-10(ok1632)* is a genomic deletion with a premature stop codon that generates an 18-aa-long protein, lacking all functional domains. Similar deletions were described as null alleles of *sel-10* (57, 60). Transgenic strains EV661 (*efIs81[Cbr-unc-119*(+) + *Pmex-5::gld-1::LAP::gld-1 3′UTR] II*), EV733 (*efIs114[Cbr-unc-119*(+) + *Pmex-5::gld-1::LAP::tbb-2 3′UTR] II*), EV735 (*efIs116[Cbr-unc-119*(+) + *Pmex-5::gld-1::LAP::oma-2 3′UTR] II*), and EV763 (*efIs124[Cbr-unc-119*(+) + *Pmex-5::GFP::H2B::sel-10 3′ UTR] II*) were generated using the Mos1-mediated single copy insertion (MosSCI) protocol (74). Injected constructs were assembled using the multisite Gateway cloning system (Thermo Fisher Scientific). To this end, the entire ORF of *gld-1* was amplified from cDNA, fused with LAP-tag encoding sequences (75) via overlap extension PCR, and inserted into the entry vector pDONR221, generating pNJ147. The *gld-1*, *oma-2*, and *sel-10* 3′UTRs were amplified from genomic DNA and inserted into pDONR-P2R-P3, resulting in entry clones pNJ81, pNJ150, and pNJ153, respectively. pCM1.36 served as a source of the *tbb-2* 3′UTR sequence (20). To generate GLD-1::LAP transgenes, pNJ147 was recombined with plasmids carrying *mex-5* promoter [pCS210 (20)], the individual 3′UTR-containing entry vectors, and the destination vector pCFJ150 (74). To generate a *sel-10* translational reporter, the PEST/GFP/H2B fusion [pBMF2.7 (20)] was recombined with pNJ153 and pCS210 into the destination vector pCFJ150, giving rise to pNJ155. All constructs were injected into the recipient strain EG6699 *ttTi5605 II; unc-119(ed3) III; oxEx1578 [eft-3p::GFP + Cbr-unc-119]*. EV375 (*ozIs5[unc-119(ed3); GLD-1::GFP] I*) was a kind gift of Tim Schedl, Washington University, St. Louis, and its use is illustrated in Fig. 2 and Fig. S1. Genotyping and cloning primers used in this study are listed in Table S1.

RNAi Feeding. Feeding RNAi experiments were performed at 20 °C according to published procedures (76) using 1 mM isopropyl-β-D(−)-thiogalactopyranoside to induce dsRNA production. Constructs targeting *sel-10* and proteasome subunits *pas-5*, *pbs-3*, *pbs-5*, and *pbs-6* were generated by PCR amplification of corresponding ORFs from cDNA with the primers listed in Table S1 and cloned into the pL4440 vector. A *cul-1* targeting construct was obtained from the RNAi library described by Kamath and Ahringer (77). The *sel-10* RNAi feedings started from the L1 stage, and all other knockdowns started from the early to mid-L4 stage.

Antibodies. Anti–GLD-1 antibodies (78) were used at a 1:1,000 dilution in Western blot analysis and at a 1:100 dilution in immunocytochemistry. Anti–OMA-1/-2 (79) was used at a dilution of 1:200, anti-FLAG (Sigma–Aldrich/Merck) at 1:5,000, anti-paramyosin MH16 antibody (Developmental Studies Hybridoma Bank) at 1:250, anti-actin (MP Biomedicals) at 1:50,000, and anti-tubulin (Sigma–Aldrich/Merck) at 1:100,000. An anti–CPB-3 monoclonal antibody (mo857A11-7) was generated at the Antibody Facility of the Max Planck Institute of Molecular Cell Biology and Genetics (MPI-CBG, Dresden, Germany) by immunizing mice with the bacterially expressed hexahistidine fusion protein of CPB-3, covering amino acids 1–281. Hybridoma supernatants were screened for strong and specific immunoreactivity in Western blotting and immunocytochemistry experiments; virtually no signal was detected in worm protein extracts or gonads of *cpb-3(tm1746)* animals. Secondary HRP-conjugated goat anti-mouse, anti-rabbit, or anti-guinea pig antibody (Jackson ImmunoResearch Laboratories) was used at a dilution between 1:20,000 and 1:40,000. Cy5-, Cy3-, or FITC-conjugated AffiniPure donkey anti-rabbit, anti-mouse, or anti-guinea pig IgG antibody (Jackson ImmunoResearch Laboratories) was used at a 1:1,000 dilution.

Immunocytochemistry and Microscopy. To extrude gonads, animals were anesthetized in a drop of M9 + 0.25 mM levamisole and quickly dissected with a 25-gauge syringe needle on a coverslip under a stereomicroscope (80). Gonads were transferred into a fixing solution of 2% paraformaldehyde (in PBS + 0.02% Tween 20) for 10 min and then permeabilized using 0.2% Triton-X in PBS for 10 min, washed three times with PBSBT (PBS + 0.5% BSA + 0.02% Tween 20), and blocked in PBSBT for at least 30 min. Incubations with antibodies and 4′,6-diamidino-2-phenylindole (DAPI; Serva) were performed largely as previously described (16). Subsequently, gonads were mounted on glass slides in Vectashield (Vector Laboratories). For in vivo imaging of GFP fusions, worms were placed on a 15-well screening slide (MP Biomedicals) and anesthetized with 0.02% sodium azide in M9 buffer. For each dataset, control animals and either RNAi or mutant animals were processed in parallel and imaged with identical exposure conditions, using an Imager M1 microscope (Zeiss) with a 63×/1.4 N.A. objective, equipped with an Axiocam MRm camera (Zeiss).

Signal Intensity Measurements. Individual images were gathered with AxioVision (Zeiss) and assembled in Fiji (ImageJ) [www.fiji.sc/ (81)]. Fluorescence intensity was measured using Fiji and analyzed in Excel (Microsoft). To measure fluorescent signal intensity around the zone of pachytene exit, Z-stack images were collected. Only images in the focal plane where the syncytium was at its maximum width were selected and stitched. A 70-pixel-wide segmented line tool that spanned about one-third of a gonad's width was used to extract intensity values from the distal tip to the proximal end. All intensity values were divided by the maximal value in a single gonad set, and are thus represented as a percentage of the maximal intensity. To determine the location of the pachytene–diplotene (P-D) border, the gross chromatin morphology of germ cell nuclei of all gonads was analyzed across several focal planes. Data points covering the selected distance (100 or 200 μm) distally and proximally from the determined P-D border were extracted and averaged.

To measure pixel intensity in selected regions of a gonad, a rectangle tool covering ∼150 μm^2 was used. Per gonad, three measurements were taken for each region of interest. Per genotype, 10 germ lines were measured and the results were averaged. Background fluorescence was determined by measuring the signal intensity of the area of the slide at some distance from mounted worms and subtracting the average background value from averages calculated for distinct gonadal regions.

Student's two-tailed *t* tests were used to examine statistical significance between average intensity differences.

Densitometry of Western blot signals was done in Fiji on scanned films using the "Gels" analysis tool (Fig. 3 *C* and *E*) or by generating a plot profile of a line scan (Fig. S4*B*).

Yeast Two-Hybrid Work. Using full-length CPB-3 as bait, a yeast two-hybrid (Y2H) screen was performed as described previously (82). For direct assays, full-length ORFs were cloned into vectors containing a LexA DNA-binding domain (DB) or Gal4 activation domain (AD), pLex or pACT, respectively (83). Whereas full-length DB::GLD-1 was found to auto-activate, full-length AD::GLD-1 was expressed at levels too low upon coexpression with DB::SEL-10 to conduct further experiments. Therefore, based on previous reports to increase hybrid protein levels (84), we removed the F-box domain from the DB::SEL-10 fusion, generating SEL-10ΔF, to prevent its likely incorporation into a functional yeast Skp, Cullin, F-box–containing complex (SCF) ubiquitin ligase complex. All proteins were verified for expression by Western blotting.

Worm Extract Preparation and Lambda Phage Phosphatase Treatment. Worm extracts were prepared by collecting hand-picked worms in M9 buffer, snap-freezing in liquid nitrogen, and subsequent boiling in Laemmli buffer. The *cpb-3(0)* extract was obtained from homozygous protein-null mutants *cpb-3 (tm1746)*. For the phosphatase assay illustrated in Fig. 3*A*, worm lysate was prepared by collecting and snap-freezing mixed-stage worms in buffer A [50 mM Tris·HCl (pH 8.9), 100 mM NaCl], and subsequent grinding in a liquid nitrogen-cooled bead mill with a 1.5-cm stainless-steel ball (Mixer Mill MM301; Retsch). To 40 mg of fine worm powder, 1 mL of 7% trichloroacetic acid (TCA; Serva) was added. The tube was briefly vortexed before centrifugation at 5,000 relative centrifugal force (rcf), 4 °C, for 10 min. Although the supernatant was discarded, the pellet was resuspended by sonication in 250 μL of buffer A supplemented with 1 mM $MnCl_2$, 1× EDTA-free cOmplete protease inhibitor mixture (Sigma), 1 μL/mL leupeptin, 1 μL/mL pepstatin, 100 μg/mL Pefabloc, 2 mM benzamidine, 1 mM PMSF, and 4 μL of 2 M Tris base to adjust the pH between 7 and 8. Aliquots of the TCA-precipitated worm extract (25 μL) were either mock-treated with 1× lambda phage phosphatase (λPP) storage buffer or additionally with 1,000 units of λPP enzyme (New England Biolabs). After incubation at 30 °C for 30 min, the reactions were stopped by the addition of 100% TCA, reaching a final

concentration of 7%. Samples were spun down at 3,000 rcf for 10 min, and only the pellet was resuspended in 20 μL of high-urea sample buffer, supplemented with 2 μL of 1 M Tris (pH 8.8) to increase the pH. Before gel separation, samples were shaken at 65 °C for 10 min and insoluble debris was spun out at 3,000 rcf for 5 min. Transfer of equal protein amounts was monitored by Ponceau staining.

Protein Biochemistry and Phos-Tag SDS/PAGE. Recombinant MBP::SEL-10 fragments and FLAG::CPB-3 or FLAG::SKR-1 fusions were coexpressed in *Spodoptera frugiperda* (Sf)+ insect cells with the help of baculoviruses as described by Rybarska et al. (83). Protein coimmunoprecipitations were performed with 25 μL of anti-FLAG resin (Sigma) in Sf+ lysis buffer as described by Rybarska et al. (83). Twenty percent of the total precipitated material was loaded on a standard SDS-Laemmli protein gel.

Phos-Tag SDS-polyacrylamide gels were generally prepared as described elsewhere (28). For the analysis of CPB-3 phosphorylation in worm lysates, 7% SDS/PAGE gel was supplemented with 5 μM Phos-Tag and 10 μM $MnCl_2$, and run in standard Laemmli 1× SDS/PAGE running buffer for 4–7 h at a constant 5–10 mA per polyacrylamide gel and a maximum of 200 V (BioRad MiniProtean system). Before blotting, Phos-Tag gels were washed twice in transfer buffer supplemented with 1 mM EDTA and twice in transfer buffer without EDTA. Proteins were blotted on ice for 3 h at a constant 400 mA and maximum 180 mA.

ACKNOWLEDGMENTS. We thank Lisette Meerstein-Kessel for the initial Y2H screen; Rafal Ciosk, Tim Schedl, and Judith Kimble for kindly providing strains and reagents; the MPI-CBG antibody facility for their help in generating antibodies; and Xico Gracida and David Rudel for comments on the manuscript. Some strains were provided by the CGC, which is funded by the NIH Office of Research Infrastructure Programs (Grant P40 OD010440). This work was financially supported by the Max Planck Society, the German Research Foundation (DFG) (Grant EC369/2-3), and the DFG Heisenberg Program (Grants EC369/3-1 and EC369/5-1 to C.R.E.).

1. Kronja I, Orr-Weaver TL (2011) Translational regulation of the cell cycle: When, where, how and why? *Philos Trans R Soc Lond B Biol Sci* 366:3638–3652.
2. Sagata N (1996) Meiotic metaphase arrest in animal oocytes: Its mechanisms and biological significance. *Trends Cell Biol* 6:22–28.
3. Von Stetina JR, Orr-Weaver TL (2011) Developmental control of oocyte maturation and egg activation in metazoan models. *Cold Spring Harb Perspect Biol* 3:a005553.
4. Richter JD, Lasko P (2011) Translational control in oocyte development. *Cold Spring Harb Perspect Biol* 3:a002758.
5. Singh G, Pratt G, Yeo GW, Moore MJ (2015) The clothes make the mRNA: Past and present trends in mRNP fashion. *Annu Rev Biochem* 84:325–354.
6. Gehring NH, Wahle E, Fischer U (2017) Deciphering the mRNP code: RNA-bound determinants of post-transcriptional gene regulation. *Trends Biochem Sci* 42:369–382.
7. Zhou HL, Geng C, Luo G, Lou H (2013) The p97-UBXD8 complex destabilizes mRNA by promoting release of ubiquitinated HuR from mRNP. *Genes Dev* 27:1046–1058.
8. Kim JH, Richter JD (2006) Opposing polymerase-deadenylase activities regulate cytoplasmic polyadenylation. *Mol Cell* 24:173–183.
9. Mendez R, et al. (2000) Phosphorylation of CPE binding factor by Eg2 regulates translation of c-mos mRNA. *Nature* 404:302–307.
10. Belloc E, Piqué M, Méndez R (2008) Sequential waves of polyadenylation and deadenylation define a translation circuit that drives meiotic progression. *Biochem Soc Trans* 36:665–670.
11. Igea A, Méndez R (2010) Meiosis requires a translational positive loop where CPEB1 ensues its replacement by CPEB4. *EMBO J* 29:2182–2193.
12. Finley D, Chen X, Walters KJ (2016) Gates, channels, and switches: Elements of the proteasome machine. *Trends Biochem Sci* 41:77–93.
13. Komander D, Rape M (2012) The ubiquitin code. *Annu Rev Biochem* 81:203–229.
14. Teixeira LK, Reed SI (2013) Ubiquitin ligases and cell cycle control. *Annu Rev Biochem* 82:387–414.
15. Hasegawa E, Karashima T, Sumiyoshi E, Yamamoto M (2006) C. elegans CPB-3 interacts with DAZ-1 and functions in multiple steps of germline development. *Dev Biol* 295:689–699.
16. Jones AR, Francis R, Schedl T (1996) GLD-1, a cytoplasmic protein essential for oocyte differentiation, shows stage- and sex-specific expression during Caenorhabditis elegans germline development. *Dev Biol* 180:165–183.
17. Francis R, Barton MK, Kimble J, Schedl T (1995) gld-1, a tumor suppressor gene required for oocyte development in Caenorhabditis elegans. *Genetics* 139:579–606.
18. Lee MH, Schedl T (2001) Identification of in vivo mRNA targets of GLD-1, a maxi-KH motif containing protein required for C. elegans germ cell development. *Genes Dev* 15:2408–2420.
19. Jungkamp A-C, et al. (2011) In vivo and transcriptome-wide identification of RNA binding protein target sites. *Mol Cell* 44:828–840.
20. Wright JE, et al. (2011) A quantitative RNA code for mRNA target selection by the germline fate determinant GLD-1. *EMBO J* 30:533–545.
21. Kimble J, Crittenden SL (2007) Controls of germline stem cells, entry into meiosis, and the sperm/oocyte decision in Caenorhabditis elegans. *Annu Rev Cell Dev Biol* 23:405–433.
22. Papaevgeniou N, Chondrogianni N (2014) The ubiquitin proteasome system in Caenorhabditis elegans and its regulation. *Redox Biol* 2:333–347.
23. Welcker M, Clurman BE (2008) FBW7 ubiquitin ligase: A tumour suppressor at the crossroads of cell division, growth and differentiation. *Nat Rev Cancer* 8:83–93.
24. Nayak S, et al. (2002) The Caenorhabditis elegans Skp1-related gene family: Diverse functions in cell proliferation, morphogenesis, and meiosis. *Curr Biol* 12:277–287.
25. Killian DJ, et al. (2008) SKR-1, a homolog of Skp1 and a member of the SCF(SEL-10) complex, regulates sex-determination and LIN-12/Notch signaling in C. elegans. *Dev Biol* 322:322–331.
26. Schmid M, Küchler B, Eckmann CR (2009) Two conserved regulatory cytoplasmic poly(A) polymerases, GLD-4 and GLD-2, regulate meiotic progression in C. elegans. *Genes Dev* 23:824–836.
27. Merritt C, Rasoloson D, Ko D, Seydoux G (2008) 3′ UTRs are the primary regulators of gene expression in the C. elegans germline. *Curr Biol* 18:1476–1482.
28. Kinoshita E, Kinoshita-Kikuta E, Takiyama K, Koike T (2006) Phosphate-binding tag, a new tool to visualize phosphorylated proteins. *Mol Cell Proteomics* 5:749–757.
29. Lapasset L, Pradet-Balade B, Lozano JC, Peaucellier G, Picard A (2005) Nuclear envelope breakdown may deliver an inhibitor of protein phosphatase 1 which triggers cyclin B translation in starfish oocytes. *Dev Biol* 285:200–210.
30. Thom G, Minshall N, Git A, Argasinska J, Standart N (2003) Role of cdc2 kinase phosphorylation and conserved N-terminal proteolysis motifs in cytoplasmic polyadenylation-element-binding protein (CPEB) complex dissociation and degradation. *Biochem J* 370:91–100.
31. Uzbekova S, et al. (2008) Spatio-temporal expression patterns of aurora kinases a, B, and C and cytoplasmic polyadenylation-element-binding protein in bovine oocytes during meiotic maturation. *Biol Reprod* 78:218–233.
32. Setoyama D, Yamashita M, Sagata N (2007) Mechanism of degradation of CPEB during Xenopus oocyte maturation. *Proc Natl Acad Sci USA* 104:18001–18006.
33. Arur S, et al. (2009) Multiple ERK substrates execute single biological processes in Caenorhabditis elegans germ-line development. *Proc Natl Acad Sci USA* 106:4776–4781.
34. Lee M-H, et al. (2007) Multiple functions and dynamic activation of MPK-1 extracellular signal-regulated kinase signaling in Caenorhabditis elegans germline development. *Genetics* 177:2039–2062.
35. Church DL, Guan KL, Lambie EJ (1995) Three genes of the MAP kinase cascade, mek-2, mpk-1/sur-1 and let-60 ras, are required for meiotic cell cycle progression in Caenorhabditis elegans. *Development* 121:2525–2535.
36. Arur S, et al. (2011) MPK-1 ERK controls membrane organization in C. elegans oogenesis via a sex-determination module. *Dev Cell* 20:677–688.
37. Detwiler MR, Reuben M, Li X, Rogers E, Lin R (2001) Two zinc finger proteins, OMA-1 and OMA-2, are redundantly required for oocyte maturation in C. elegans. *Dev Cell* 1:187–199.
38. de la Cova C, Greenwald I (2012) SEL-10/Fbw7-dependent negative feedback regulation of LIN-45/Braf signaling in C. elegans via a conserved phosphodegron. *Genes Dev* 26:2524–2535.
39. Kong J, Lasko P (2012) Translational control in cellular and developmental processes. *Nat Rev Genet* 13:383–394.
40. Glisovic T, Bachorik JL, Yong J, Dreyfuss G (2008) RNA-binding proteins and post-transcriptional gene regulation. *FEBS Lett* 582:1977–1986.
41. Nousch M, Eckmann CR (2012) Translational control in the Caenorhabditis elegans germ line. *Advances in Experimental Medicine and Biology* (Springer, New York), pp 205–247.
42. Zimyanin V, Lowe N, St Johnston D (2007) An oskar-dependent positive feedback loop maintains the polarity of the Drosophila oocyte. *Curr Biol* 17:353–359.
43. Horvay K, Claussen M, Katzer M, Landgrebe J, Pieler T (2006) Xenopus Dead end mRNA is a localized maternal determinant that serves a conserved function in germ cell development. *Dev Biol* 291:1–11.
44. Yang C-K, Yen P (2013) Differential translation of Dazap1 transcripts during spermatogenesis. *PLoS One* 8:e60873.
45. Lublin AL, Evans TC (2007) The RNA-binding proteins PUF-5, PUF-6, and PUF-7 reveal multiple systems for maternal mRNA regulation during C. elegans oogenesis. *Dev Biol* 303:635–649.
46. Lamont LB, Crittenden SL, Bernstein D, Wickens M, Kimble J (2004) FBF-1 and FBF-2 regulate the size of the mitotic region in the C. elegans germline. *Dev Cell* 7:697–707.
47. Inoue D, Ohe M, Kanemori Y, Nobui T, Sagata N (2007) A direct link of the Mos-MAPK pathway to Erp1/Emi2 in meiotic arrest of Xenopus laevis eggs. *Nature* 446:1100–1104.
48. Keady BT, Kuo P, Martínez SE, Yuan L, Hake LE (2007) MAPK interacts with XGef and is required for CPEB activation during meiosis in Xenopus oocytes. *J Cell Sci* 120:1093–1103.
49. Sha Q-Q, et al. (2017) A MAPK cascade couples maternal mRNA translation and degradation to meiotic cell cycle progression in mouse oocytes. *Development* 144:452–463.
50. Nabti I, Marangos P, Bormann J, Kudo NR, Carroll J (2014) Dual-mode regulation of the APC/C by CDK1 and MAPK controls meiosis I progression and fidelity. *J Cell Biol* 204:891–900.
51. Dupré A, Haccard O, Jessus C (2011) Mos in the oocyte: How to use MAPK independently of growth factors and transcription to control meiotic divisions. *J Signal Transduct* 2011:350412.

52. Minshall N, Reiter MH, Weil D, Standart N (2007) CPEB interacts with an ovary-specific eIF4E and 4E-T in early Xenopus oocytes. *J Biol Chem* 282:37389–37401.
53. Sette C (2010) Post-translational regulation of STAR proteins and effects on their biological functions. *Germ Cell Development in C. elegans*, ed Schedl T (Springer, Boston), pp 54–66.
54. Matter N, Herrlich P, König H (2002) Signal-dependent regulation of splicing via phosphorylation of Sam68. *Nature* 420:691–695.
55. Paronetto MP, et al. (2006) The nuclear RNA-binding protein Sam68 translocates to the cytoplasm and associates with the polysomes in mouse spermatocytes. *Mol Biol Cell* 17:14–24.
56. Tetzlaff MT, et al. (2004) Defective cardiovascular development and elevated cyclin E and Notch proteins in mice lacking the Fbw7 F-box protein. *Proc Natl Acad Sci USA* 101:3338–3345.
57. Jäger S, Schwartz HT, Horvitz HR, Conradt B (2004) The Caenorhabditis elegans F-box protein SEL-10 promotes female development and may target FEM-1 and FEM-3 for degradation by the proteasome. *Proc Natl Acad Sci USA* 101:12549–12554.
58. Hubbard EJ, Wu G, Kitajewski J, Greenwald I (1997) sel-10, a negative regulator of lin-12 activity in Caenorhabditis elegans, encodes a member of the CDC4 family of proteins. *Genes Dev* 11:3182–3193.
59. Ding M, Chao D, Wang G, Shen K (2007) Spatial regulation of an E3 ubiquitin ligase directs selective synapse elimination. *Science* 317:947–951.
60. Peel N, Dougherty M, Goeres J, Liu Y, O'Connell KF (2012) The C. elegans F-box proteins LIN-23 and SEL-10 antagonize centrosome duplication by regulating ZYG- 1 levels. *J Cell Sci* 125:3535–3544.
61. Ou C-Y, Lin Y-F, Chen Y-J, Chien C-T (2002) Distinct protein degradation mechanisms mediated by Cul1 and Cul3 controlling Ci stability in Drosophila eye development. *Genes Dev* 16:2403–2414.
62. Gutierrez GJ, et al. (2006) Meiotic regulation of the CDK activator RINGO/Speedy by ubiquitin-proteasome-mediated processing and degradation. *Nat Cell Biol* 8: 1084–1094.
63. Wertz IE, et al. (2011) Sensitivity to antitubulin chemotherapeutics is regulated by MCL1 and FBW7. *Nature* 471:110–114.
64. Inuzuka H, et al. (2011) Mcl-1 ubiquitination and destruction. *Oncotarget* 2:239–244.
65. Zhong Q, Gao W, Du F, Wang X (2005) Mule/ARF-BP1, a BH3-only E3 ubiquitin ligase, catalyzes the polyubiquitination of Mcl-1 and regulates apoptosis. *Cell* 121: 1085–1095.
66. Ding Q, et al. (2007) Degradation of Mcl-1 by beta-TrCP mediates glycogen synthase kinase 3-induced tumor suppression and chemosensitization. *Mol Cell Biol* 27: 4006–4017.
67. Bohnert KA, Kenyon C (2017) A lysosomal switch triggers proteostasis renewal in the immortal C. elegans germ lineage. *Nature* 551:629–633.
68. Ivshina M, Lasko P, Richter JD (2014) Cytoplasmic polyadenylation element binding proteins in development, health, and disease. *Annu Rev Cell Dev Biol* 30:393–415.
69. Tay J, Hodgman R, Richter JD (2000) The control of cyclin B1 mRNA translation during mouse oocyte maturation. *Dev Biol* 221:1–9.
70. de Moor CH, Richter JD (1999) Cytoplasmic polyadenylation elements mediate masking and unmasking of cyclin B1 mRNA. *EMBO J* 18:2294–2303.
71. Lee M-H, Schedl T (2010) C. elegans star proteins, GLD-1 and ASD-2, regulate specific RNA targets to control development. *Adv Exp Med Biol* 693:106–122.
72. Sánchez F, Smitz J (2012) Molecular control of oogenesis. *Biochim Biophys Acta* 1822: 1896–1912.
73. Brenner S (1974) The genetics of Caenorhabditis elegans. *Genetics* 77:71–94.
74. Frøkjær-Jensen C, Davis MW, Ailion M, Jorgensen EM (2012) Improved Mos1-mediated transgenesis in C. elegans. *Nat Methods* 9:117–118.
75. Sarov M, et al. (2012) A genome-scale resource for in vivo tag-based protein function exploration in C. elegans. *Cell* 150:855–866.
76. Kamath RS, Martinez-Campos M, Zipperlen P, Fraser AG, Ahringer J (2001) Effectiveness of specific RNA-mediated interference through ingested double-stranded RNA in Caenorhabditis elegans. *Genome Biol* 2:RESEARCH0002.
77. Kamath RS, Ahringer J (2003) Genome-wide RNAi screening in Caenorhabditis elegans. *Methods* 30:313–321.
78. Jan E, Motzny CK, Graves LE, Goodwin EB (1999) The STAR protein, GLD-1, is a translational regulator of sexual identity in Caenorhabditis elegans. *EMBO J* 18: 258–269.
79. Nousch M, Techritz N, Hampel D, Millonigg S, Eckmann CR (2013) The Ccr4-Not deadenylase complex constitutes the main poly(A) removal activity in C. elegans. *J Cell Sci* 126:4274–4285.
80. Crittenden SL, Troemel ER, Evans TC, Kimble J (1994) GLP-1 is localized to the mitotic region of the C. elegans germ line. *Development* 120:2901–2911.
81. Schindelin J, et al. (2012) Fiji: An open-source platform for biological-image analysis. *Nat Methods* 9:676–682.
82. Kraemer B, et al. (1999) NANOS-3 and FBF proteins physically interact to control the sperm-oocyte switch in Caenorhabditis elegans. *Curr Biol* 9:1009–1018.
83. Rybarska A, et al. (2009) GLS-1, a novel P granule component, modulates a network of conserved RNA regulators to influence germ cell fate decisions. *PLoS Genet* 5: e1000494.
84. Starostina NG, et al. (2007) A CUL-2 ubiquitin ligase containing three FEM proteins degrades TRA-1 to regulate C. elegans sex determination. *Dev Cell* 13:127–139.